

# A Hybrid Patient-Specific Biomechanical Model Based Image Registration Method for the Motion Estimation of Lungs

Lianghao Han<sup>a,\*</sup>, Hua Dong<sup>b,\*</sup>, Jamie McClelland<sup>d</sup>, L.X. Han<sup>c</sup>, David Hawkes<sup>d</sup>, Dean Barratt<sup>d</sup>

<sup>a</sup>Shanghai East Hospital, School of Medicine, Tongji University, 1239 Siping Road, Shanghai, P.R. China

<sup>b</sup>College of Design and Innovation, Tongji University, 1239 Siping Road, Shanghai P.R. China

<sup>c</sup>School of Computing, Mathematics and Digital Technology, Manchester Metropolitan University, Chester Street, Manchester M1 5GD, UK

<sup>d</sup>Centre for Medical Image Computing, University College London, Gower Street, London, WC1E 6BT, UK

---

## Abstract

This paper presents a new hybrid biomechanical model-based deformable image registration method for lung motion estimation. In the proposed method, a patient-specific biomechanical modelling process captures major physically plausible deformations with explicitly physical modelling of sliding motion, whilst a subsequent non-rigid image registration process compensates for small residuals. The proposed algorithm was evaluated with 10 4D CT datasets of lung cancer patients. The target registration error (TRE), defined as the Euclidean distance of landmark pairs, was significantly lower with the proposed method (TRE=1.37mm) than with biomechanical model (TRE=3.81) and intensity-based image registration without specific considerations for sliding motion (TRE=4.57mm). The proposed method achieved comparable accuracies as several recently developed intensity-based registration algorithms with sliding handling on the same datasets. A detailed comparison on the distributions of TREs with three non-linear intensity-based algorithms showed that the proposed method performed especially well on estimating the displacement field of lung surface regions (mean TRE = 1.33mm, maximum TRE = 5.3mm). The effects of biomechanical model parameters, Poisson's ratio, friction and tissue heterogeneity, on displacement estimation were investigated. The potential of the algorithm in optimising biomechanical models through analysing the pattern of displacement compensation from the image registration process has also been demonstrated.

13 *Keywords:* Sliding motion, Biomechanical modelling, Finite element method, Image  
14 registration, 4D CT, Lung

---

## 15 **1. Introduction**

16 Respiratory motion can cause artefacts in images during thorax and abdomen imag-  
17 ing. Accurate estimation and correction for the effects of respiratory motion can poten-  
18 tially increase the applications of medical images in diagnosis, treatment planning and  
19 image-guided interventions etc. (McClelland et al., 2013). A wide range of different  
20 techniques including biomechanical models, intensity-based image registration or hybrid  
21 methods have been proposed for estimating lung motion (Murphy et al., 2011; Fuerst  
22 et al., 2015), but most research efforts are put on intensity-based image registration  
23 techniques.

### 24 *1.1. Intensity-based image registration methods for lung motion estimation*

25 One of the challenges for estimating lung motion with non-rigid intensity-based image  
26 registration techniques is to handle with the sliding motion of lungs against adjacent  
27 structures such as rib cage and diaphragm, which produces a non-smooth, discontinuous  
28 displacement field at sliding interfaces. The intensity-based image registration methods  
29 commonly incorporate smoothness conditions on the voxel displacement field in order  
30 to ensure deformation consistency. Such smoothing constraints are good approximations  
31 within deformable, soft tissue organs, but are strictly not valid at tissue boundaries where  
32 sliding occurs.

33 One solution to this problem is to generate masks with image segmentation for sep-  
34 arating two anatomic regions in relative motion and register the two regions separately  
35 (Rietzel and Chen, 2006; Vandemeulebroucke et al., 2012). In this way, direct handling  
36 of sliding motion is avoided and standard (intensity-based) algorithms can be used with  
37 no or very little modification. However, one problem with this approach is that gaps

---

\*Corresponding author

*Email addresses:* [lhhan@tongji.edu.cn](mailto:lhhan@tongji.edu.cn) (Lianghao Han), [donghua@tongji.edu.cn](mailto:donghua@tongji.edu.cn) (Hua Dong),  
[l.han@mmu.ac.uk](mailto:l.han@mmu.ac.uk) (L.X. Han), [d.hawkes@ucl.ac.uk](mailto:d.hawkes@ucl.ac.uk) (David Hawkes), [d.barratt@ucl.ac.uk](mailto:d.barratt@ucl.ac.uk) (Dean Barratt)

38 and overlaps between nearby voxels may appear near the sliding interfaces. To reduce  
39 or eliminate gaps between the independently registered regions, a boundary-matching  
40 penalty method has been proposed in which an artificial uniform band with a unique  
41 intensity value around the sub-regions is added (McClelland et al., 2006; Wu et al.,  
42 2008; Vandemeulebroucke et al., 2012). This has the effect of creating a strong spa-  
43 tial gradient around the sliding interface, which guides each registration, resulting in  
44 greater consistency at the interfaces. An alternative approach is to incorporate a spe-  
45 cific regularisation of sliding motion into the registration optimisation. Such schemes  
46 are mainly based on the consideration that the deformation components in the nor-  
47 mal and tangential directions near to sliding boundaries have different contributions to  
48 sliding motion; the sliding behaviour is mainly controlled by the tangential component.  
49 For example, Schemit-Richberg et al. (Schmidt-Richberg et al., 2012a,b) described a  
50 direction-dependent diffusion regularisation approach. In their method, the tangential  
51 component was smoothed separately for the two adjacent regions on either side of their  
52 common sliding interfaces, whilst the normal component was smoothed jointly across  
53 the two regions. This allows a discontinuous movement between the two sub-regions in  
54 the tangential direction but maintains smoothness in the normal direction to reduce gaps  
55 and overlaps. Similarly, Delmon et al. (Delmon et al., 2013) proposed a B-spline registra-  
56 tion method with direction-dependent B-spline decomposition for sliding regularisation.  
57 They used a B-spline transformation for each sub-region to capture the discontinuities  
58 of displacement due to sliding motion between two sub-regions. Pace et al. (Pace et al.,  
59 2011) presented an anisotropic diffusive regularisation method in which separate nonlin-  
60 ear anisotropic smoothing filters were applied to the normal and tangential deformation  
61 components of displacement. More recently, Riser et al. (Risser et al., 2013) proposed a  
62 direction-dependent regularisation within a diffeomorphic registration framework, similar  
63 to Schemit-Richberts methods. However, they decomposed the velocity field rather than  
64 the displacement field into normal and tangential components. To consider discontinu-  
65 ities of deformation existing in both normal and tangent directions around boundaries  
66 between lung lobe fissures, Yin et al. (Yin et al., 2010) used a diffusive regularisation with  
67 an additional distance weighting term increasing with the distance to the organ bound-  
68 ary. This ensures that the displacement discontinuity characteristics of sliding motion

69 near organ boundaries are not penalized.

70 All the above methods require segmenting sliding structures in the images to be reg-  
71 istered. To address this pre-requisite, Schemit-Richberg et al. (Schmidt-Richberg et al.,  
72 2012b) extended their method, demonstrating that it was possible to automatically de-  
73 tect sliding organs, thus removing the requirement for prior image segmentation which  
74 may be impractical or overly time-consuming for some clinical applications. Several  
75 intensity-based image regularisation methods that do not require a prior segmentation  
76 have also been proposed to preserve sliding motion. Based on the decomposition of the  
77 displacement vector, Ruan et al. (Ruan et al., 2009), for instance, proposed a regular-  
78 isation energy function written as a combination of an L2 norm of the divergence of  
79 the displacement vector (i.e. the relative variation of the volume) and an L1 norm of  
80 a rotational vector (i.e. the curl of the displacement field). Penalizing the L2 norm  
81 conserves the volume change, whilst penalizing the L1 norm preserves large shear along  
82 the boundaries. Further, Heinrich et al. (Heinrich et al., 2010) showed that a non-  
83 quadratic regularisation using the  $L_p$  norm ( $p \leq 1$ ) can preserve the sliding motion  
84 of lungs within an optical flow based registration algorithm. More recently, Heinrich et  
85 al. (Heinrich et al., 2013) introduced an intensity-derived minimum-spanning tree into  
86 their Markov random field (MRF) based deformable registration method to represent the  
87 underlying structure of the anatomical connectivity of the image. A pair-wise regularisa-  
88 tion acts only on connections (edges) between two nodes of the tree. Using this method,  
89 the sliding motion is preserved. However, since sliding motion is not handled explicitly,  
90 all of these methods require large variations of image gradient at the sliding boundaries  
91 in order to preserve the sliding motion. Therefore, such regularisation approaches may be  
92 insufficient when the image intensities are similar near the interface between two sliding  
93 objects; for example, at the boundary between the chest wall and the liver in CT or MR  
94 images.

### 95 *1.2. Biomechanical model based methods for lung motion estimation*

96 Biomechanical modelling is another commonly used approach for estimating lung  
97 motion. In the biomechanical modelling techniques, the sliding motion between two  
98 anatomic structures is often treated as a frictional or frictionless contact problem, which  
99 then is solved using finite element (FE) methods. Zhang et al. (Zhang et al., 2004)

100 proposed a deformable lung FE model with pleural sliding using contact elements in the  
101 commercial FE package ANSYS (<http://www.ansys.com>). Lung expansion from the end  
102 exhalation to the end inhalation was simulated by applying a negative uniform pressure  
103 to the external lung surface until it fills the chest cavity; the interaction between the lungs  
104 and their surrounding body was modelled explicitly as a contact problem. The feasibility  
105 of this approach was demonstrated by using two 3D breathhold lung CT images, acquired  
106 from one patient at the exhalation phase and at the deep inspiration phase. Villard et  
107 al. (Villard et al., 2005) described a similar FE model for deformable lung registration.  
108 Pleural sliding between the rib cage and lungs was modelled as a frictionless contact us-  
109 ing the open source FE software toolkit, Code\_Aster ([www.code-aster.org](http://www.code-aster.org)). Following  
110 the ideas of Zhang and Villard on lung FE models, Werner et al. (Werner et al., 2009a)  
111 simulated the lung expansion under a negative pressure using the commercial FE soft-  
112 ware package, COMOSOL *Multiphysics* (<http://www.comsol.ltd.uk>), and provided  
113 a detailed quantitative evaluation of their lung model using CT datasets from 12 lung  
114 tumour patients. The results suggested that an FE modelling approach was adequate in  
115 predicting lung dynamics due to lung ventilation, even lung tissue was assumed to be an  
116 isotropic, homogeneous and linearly elastic material. More recently, Fuerst et al. (Fuerst  
117 et al., 2015) simulated the lung expansion from the end-exhale to the end-inspiration  
118 by applying different negative pressures on the pre-defined surface zones of thorax and  
119 diaphragm contacting with lungs, respectively. The applied pressures were then trans-  
120 formed to the lung surface through a lung/thorax/diaphragm interaction model, whose  
121 values were estimated through an optimisation procedure where the model-estimated  
122 lung change was compared to CT images at end-inspiration. The sliding between the  
123 lung and the surfaces of thorax cavity and diaphragm was simulated as a frictionless  
124 contact problem.

125 **Bioemchanial modelling of lung respiration has also been treated as a compression**  
126 **process from inspiration to expiration.** Using a frictionless contact model, Al-Mayah et  
127 al. (Al-Mayah et al., 2008) modelled the lung sliding against the chest cavity using the  
128 commercial FE software package, ABAQUS (<http://www.3ds.com>). In this case, they  
129 simulated lung respiration as a compression process from inspiration to expiration by ap-  
130 plying displacement boundary conditions to the inner surface of the chest cavity directly

131 in contact with the lung surface. They used the commercial mesh manipulation tool,  
132 Hypermorph (<http://www.altairhyperworks.com>), to deform the surface mesh of the  
133 chest cavity at end inhalation to match the surface mesh at end-exhalation, and obtain  
134 the displacements of each node on the surface mesh of the chest cavity at end inhala-  
135 tion. These nodal displacements were then used as displacement boundary conditions  
136 to deform the lungs in the FE models. Using similar FE models, they investigated the  
137 effects of friction near the interface (Al-Mayah et al., 2009), the heterogeneity of lung  
138 structures (Al-Mayah et al., 2010), linear/nonlinear material models (Al-Mayah et al.,  
139 2008) and material parameters of lung tissues (Al-Mayah et al., 2009).

140 Compared to intensity-based image registration techniques, biomechanical modelling  
141 often has lower requirements for image quality and can work on noisy images, such  
142 as ultrasound, since the generation of biomechanical models in many applications only  
143 requires organ surface data from images. Another attractive feature is that biome-  
144 chanical modelling can provide an integrated solution in one single model for physics  
145 and physiology based lung motion, including but not limited to predicting the deforma-  
146 tion/motion of tumor, evaluating the effect of gravity on respiratory physiology, simulate  
147 bio-physiological processes, such as respiratory motion, and provide physically realistic  
148 sliding motion, including explicitly information on physical properties and mechanical  
149 behaviour of anatomical structures, with or without pathology, if they are available;  
150 such an integrated scheme is unknown for non-rigid image registration techniques. How-  
151 ever, due to various uncertainties, such as forces exerted by the beating heart, variable  
152 lung and blood pressure, and variable mechanical properties of *in vivo* tissues, which are  
153 in general very difficult to measure accurately, combined with limited tissue contrast in  
154 some image modalities and limited computational time and resources, a number of sim-  
155 plifications and assumptions are required when generating biomechanical models. Unlike  
156 image-intensity based image registration methods, it is also extremely difficult, if not  
157 impossible, for biomechanical models to include very detailed internal tissue structures  
158 whose deformations may directly manifest as intensity changes in medical images. All  
159 of these factors limit the accuracy of biomechanical models in predicting displacement  
160 distributions of tissue structures. Previous lung motion studies show that biomechanical  
161 models only achieve equivalent prediction accuracy as intensity-based image registration

162 methods without sliding motion regularisation, but exhibit inferior registration perfor-  
163 mance compared with intensity-based image registration methods with sliding regularisa-  
164 tion in terms of landmark-based TRE (Werner et al., 2009a,b). Therefore, intensity-based  
165 image registration methods and biomechanical modelling have their own advantages and  
166 disadvantages when applied to lung motion estimation involving interface sliding, but an  
167 important observation that underlies the work described in the present paper is that the  
168 advantages of these methods are potentially complementary.

169 Previous studies (Li et al., 2008; Han et al., 2014b; Samavati et al., 2015; Hipwell  
170 et al., 2016) have shown that a combined method integrating intensity-based registra-  
171 tion with biomechanical modelling can compensate physically unrealistic estimated tissue  
172 motion (Li et al., 2008), reduce the uncertainty of biomechanical modelling ((Samavati  
173 et al., 2015)), compensate displacement residuals ((Han et al., 2014b)) due to the simpli-  
174 fication of biomechanical models, and improve the registration performance by increasing  
175 image overlap (Han et al., 2014b; Hipwell et al., 2016). Our recent preliminary studies  
176 on deformable registration of CT lung images have demonstrated a good registration  
177 performance using a combined method (Han et al., 2014a) , in which an intensity-based  
178 image registration process provides a displacement compensation to displacement residues  
179 of biomechanical modelling. Since the displacement compensation reflects the distribu-  
180 tions of the prediction errors of biomechanical modelling, which potentially could be used  
181 to provide directions for optimising model parameters and constructing more accurate  
182 predictive biomechanical models..

183 In the present study, we propose a patient-specific, hybrid biomechanical model-based  
184 image registration method for lung motion estimation, as an extension of the work re-  
185 ported in (Han et al., 2014a). In this method, a biomechanical modelling process with  
186 an FE method estimates the major component of the deformation field from a source  
187 image to a target image which is then used to warping the source image to obtain an  
188 FE-estimated target image, and then the FE-estimated target image is registered to the  
189 target image in a subsequent non-rigid image registration process to compensate rela-  
190 tively small residuals of displacement due to simplifications and uncertainty in the model  
191 parameters that are inherent in the biomechanical models. This has the advantages  
192 that the deformation recovered by the image registration algorithm is relatively small.

193 The accuracy of the proposed method was tested using publicly available **annotated** 4D  
194 CT datasets of 10 lung cancer patients from the DIR-lab database (www.dir-lab.com)  
195 (Castillo et al., 2009). The effects of FE model parameters on the accuracy of biome-  
196 chanical modelling in lung motion estimation and the potential of the pattern analysis of  
197 displacement compensation in optimising biomechanical models were also investigated.

198 The main contributions of the study are in **(1) developing a biomechanical model**  
199 **based non-rigid image registration method that can not only have a comparable registra-**  
200 **tion performance with the state-of-the-art intensity-based non-rigid image registration**  
201 **methods but also can provide physically realistic deformation estimations with an in-**  
202 **tegrated solution for various physiological properties modelling of the lungs in a single**  
203 **FE model**, and **(2) demonstrating that the proposed method has the potential to be**  
204 **used for guiding the improvement of biomechanical models through analysing the pat-**  
205 **tern of displacement compensation from the intensity-based non-rigid image registration**  
206 **process.**

## 207 **2. Methods and Materials**

208 In this study, we demonstrated and evaluated the proposed registration method  
209 through estimating lung motion from the end-exhale to the end-inspiration, that is,  
210 determining the transformation/displacement between two images (a source image and  
211 a target image), which correspond to the two breath phases, respectively.

### 212 *2.1. Hybrid biomechanical model based image registration method*

213 Figure 1 illustrates the proposed image registration method, which includes two con-  
214 secutive processes: (1) patient-specific biomechanical modelling of lung motion, and (2)  
215 intensity-based image registration.

216 The biomechanical modelling process consists of two main steps: i) construct a  
217 patient-specific biomechanical model based on the geometry models extracted from CT  
218 images ii) perform biomechanical modelling to estimate displacement fields of the anatomic  
219 structures, and then use them to warp the source image to generate an **FE**-estimated  
220 target image. Immediately after the biomechanical modelling process, the intensity-  
221 based image registration process is then used to determine the transformations applied



222 to the **FE**-estimated target image in order to align it with the target image. Since im-  
 223 age registration is between the **FE**-estimated target image and the target image, the  
 224 transformations obtained are essentially the displacement compensation to the initial  
 225 biomechanical-model-estimated displacement field. The estimated total displacement  
 226 field relating the source image to the target image is now the sum of the estimated dis-  
 227 placements from the biomechanical modelling process and the displacements determined  
 from the intensity-based image registration process.

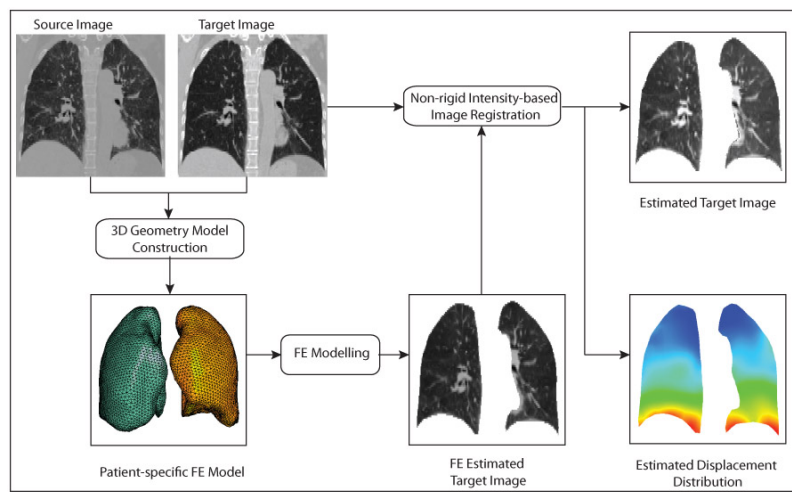


**Figure 1:** Biomechanical-model based image registration framework

228

229 *2.2. Biophysical process of lung respiratory motion*

230 To build a biomechanical model of lungs for motion estimation, a basic understanding  
 231 of anatomy and mechanics of the compression and expansion procedure during respiration  
 232 is needed. As shown in Fig. 2, the human lungs are situated in the thoracic cavity, with  
 233 each lung is surrounded by a pleural cavity consisting of two pleurae: the parietal pleura  
 234 and the visceral pleura. The parietal pleura is attached to the internal walls of the  
 235 thoracic cavity (i.e. rib cage) and the diaphragm, whilst the visceral pleura covers the  
 236 surfaces of the lungs. The space between the two layers is the pleural cavity containing  
 237 a thin film of pleural fluid. The pleural fluid lubricates the inside surfaces of the pleural  
 238 cavity, allowing the parietal and visceral pleurae to slide smoothly over one another  
 239 during respiration. It also provides surface tension to keep the lung surfaces in contact

with the chest wall.

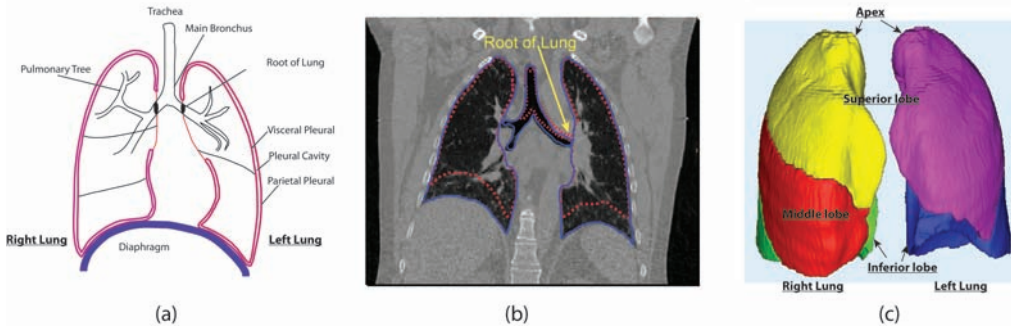


**Figure 2:** (a) Schematic diagram of lung anatomy; (b) lung contours at full expiration and full inspiration, superimposed on a coronal slice of a 3D CT volume (Case1); (c) lung lobes segmented from the CT volume. The dashed lines in red and the solid lines in blue shown in Fig. 2(b) correspond to the lung contours at the full expiration and full inspiration, respectively.

240

241 The lung is connected to the heart and the trachea by the root of the lung, which  
 242 is surrounded by pleurae and connects the medial surface of each lung to the heart and  
 243 trachea (Gray, 1918). The lower end and the bifurcation of the trachea are displaced  
 244 downwards during inspiration, and the lung expands in a downward and forward direc-  
 245 tion. The roots of the lungs descend to facilitate this motion. Fig. 2(b) illustrates that  
 246 the lung roots at full expiration are higher than their positions at full inspiration.

247 During inspiration, the contraction and the downward movement of the diaphragm  
 248 cause an increase in thoracic volume and a decrease in pleural and alveolar pressures;  
 249 consequently, the lungs expand and air is drawn in. During expiration, the relaxation  
 250 and the upward movement of the diaphragm result in the decrease of thoracic volume and  
 251 the increase of pleural pressure, the lungs spring back to their original positions and air  
 252 flows out. The pleural pressure is always negative during normal breathing (Gray, 1918),  
 253 and the visceral pleura slides against the parietal pleura. Therefore, the respiratory  
 254 motion of the lung could be modelled by applying a negative pressure to the lung, and  
 255 the interaction between the lungs and the pleural cavity could be considered as a contact  
 256 problem (Zhang et al., 2004; Villard et al., 2005; Werner et al., 2009a).

257 *2.3. Patient-specific biomechanical modelling of lung motion*

258 Biomechanical modelling for lung motion estimation starts from simulating the lung  
259 deformation between two respiratory phases. Under a negative pressure, a deformable  
260 lung model at its initial state, corresponding to the first respiratory phase, is expanded  
261 to its target volume corresponding to the second respiratory phase. The surfaces of the  
262 target volume limit the final deformation of the lung model. To generate a patient-specific  
263 biomechanical model of a lung, its 3D geometries at the two phases are required. In this  
264 study, they were extracted from 4D CT data using a four-step segmentation process as  
265 follows:

- 266 Step 1. Extract lung regions (including the trachea and airways) using a semi-automatic  
267 segmentation method consisting of region competition and level set snake evolu-  
268 tion (Yushkevich et al., 2005).
- 269 Step 2. Extract the masks of trachea and large airways using the same segmentation  
270 process.
- 271 Step 3. Remove the masks of trachea and airways from the lung segmentation masks  
272 obtained in Step 1 to separate the left and right lungs.
- 273 Step 4. Generate closed lung segmentation masks with opening and closing operation.

274 Normally, the masks of left and right lungs can be separated automatically after Step  
275 3. If the junctions between them are thin and have weak intensity contrast within the  
276 images, the separation of the left and right lungs can be performed manually. This is the  
277 case for Case 2 and Case 8. The lung volumes following segmentation are summarized  
278 in Table 1.

279 After lungs have been segmented, an automatic FE model generation process (Han  
280 et al., 2012) is used to generate an FE model. A previous study (Amelon, 2012) has  
281 shown that the accuracy of FE simulations was not affected by including the lobar slid-  
282 ing intra-lobar sliding for 4D CT image registration. Therefore, in this study, we only  
283 consider the sliding motion between the entire lung and the chest wall. The FE model  
284 of the lungs (Han et al., 2014a) includes deformable lungs extracted from the lung seg-  
285 mentation of 3D CT images at end exhale, and rigid surfaces extracted from the lung  
286 segmentation of 3D CT images at full-inspiration. First-order linear interpolation tetra-  
287 hedral and second-order quadratic elements are two basic types of elements used in

**Table 1:** Lung Volumes of 10 Patients (in litre)

Subject No	Volume at full expiration( $l$ )		Volume at full inspiration( $l$ )		Volume ratio(%)	
	left	right	left	right	left	right
Case 1	0.95	1.26	1.00	1.37	5.46	9.15
Case 2	2.32	2.68	2.58	2.96	10.91	10.33
Case 3	1.73	1.98	1.94	2.25	11.97	13.14
Case 4	1.14	1.53	1.32	1.74	16.02	13.65
Case 5	1.41	1.72	1.55	1.93	9.94	12.60
Case 6	1.12	1.36	1.40	1.76	24.31	29.96
Case 7	1.40	1.70	1.73	2.07	23.23	21.38
Case 8	2.25	2.46	2.66	3.02	18.00	22.43
Case 9	0.76	0.93	0.90	1.08	17.41	16.27
Case 10	1.16	1.76	1.36	2.04	17.71	15.89
Mean(SD)	1.42(0.5)	1.74(0.5)	1.64(0.6)	2.02(0.6)	15.5(5.9)	16.5(6.4)

288 FE-based image registration methods, a previous study (Al-Mayah et al., 2011) on lung  
289 motion simulations has shown little difference between the models of the two types of  
290 tetrahedral elements. In this study, the deformable lungs are meshed with 4-node tetra-  
291 hedron elements and the rigid surfaces are meshed with 3-node triangular shell elements.  
292 The rigid surfaces are used as constraints to limit the deformation of the deformable  
293 lungs, and all 6 degrees of freedoms (DOF) of the nodes on the rigid surfaces are fixed  
294 to prevent rigid-body motions. To simulate the sliding motion of the pleurae against the  
295 chest wall, contact pairs are defined between the surface of the deformable lungs and the  
296 rigid surfaces, with or without friction.

297 The lung parenchyma is assumed to be a compressible, nonlinearly elastic, homo-  
298 geneous continuum, modelled with a two-parameter Neo-Hookean model. The strain  
299 energy function for describing the Neo-Hookean model,  $W$ , is defined as

$$W = C_{10}(\bar{I}_1 - 3) + \frac{1}{D_1}(J^{el} - 1)^2 \quad (1)$$

300 where  $\bar{I}_1$  is the first deviatoric strain invariant associated with deviatoric stretches,  $J^{el}$   
 301 is the elastic Jacobian, and  $C_{10}$  and  $D_1$  are two material parameters which are related to  
 302 initial shear modulus,  $\mu_0$ , and initial bulk modulus,  $K_0$ , at small strain, by the relations:

$$\mu_0 = 2C_{10}, K_0 = \frac{2}{D_1} \quad (2)$$

304 where  $\mu_0$ , and  $K_0$  are related to two commonly used infinitesimal elasticity parame-  
 305 ters, Young's modulus,  $E$ , and Poisson's ratio,  $\nu$ , through the relations:

$$\mu_0 = \frac{E}{2(1+\nu)} \quad (3)$$

306

$$K_0 = \frac{E}{3(1-2\nu)} \quad (4)$$

307 Thus, the NeoHookean hyperelastic model can be defined by Young's modulus and Pois-  
 308 son's ratio. Due to a lack of *in vivo* data on mechanical properties of lungs, different  
 309 values ranging from 0.1 kPa to 7.8 kPa for Young's modulus, and from 0.2 to 0.45 for  
 310 the Poisson's ratio, based on *in vitro* experimental data from dog or human or arbitrary  
 311 choices, have been used in previous lung studies (Werner et al., 2009a).

312 In this study, we assume that lungs are homogeneous in the sense that there is no  
 313 difference in mechanical properties between different lobes (unless otherwise specifically  
 314 stated). Because of the final shape constraint and the homogeneity assumption, the  
 315 changes of material parameters (Young's modulus and Poisson's ratio) have little effect  
 316 on displacement distribution after the lung is expanded to its target volume (Werner  
 317 et al., 2009a); they only affect the value of pleural pressure required to fully inflate the  
 318 lung to the target volume. A stiffer lung tissue and a higher value of Poisson's ratio  
 319 require a higher pleural pressure and a longer computation time if implicit integration  
 320 schemes are used in the FE modelling. Based on literature values, a reference value of 5  
 321 kPa and 0.2 are chosen for Young's modulus and Poisson's ratio, respectively.

322 With the specified material parameters, the minimum pleural pressure required to  
 323 expand a lung to its target volume could be estimated from the definition of bulk modulus  
 324 (Villard et al., 2005). Bulk modulus,  $K$ , is a measure of the substance's resistance to  
 325 uniform compression defined as the ratio of the infinitesimal pressure increase to the

326 resulting relative decrease of the volume.

$$K = -V_0 \times \frac{dP}{dV} \quad (5)$$

327 where  $V_0$  is the initial volume of the lung,  $dP$  and  $dV$  are the difference in pleural pressure  
328 and the difference in lung volume at two different breathing phases, respectively. The  
329 inverse of the bulk modulus gives the lung's compressibility, which can be expressed as:

$$\frac{1}{K} = -\frac{1}{V_0} \times \frac{dV}{dP} \quad (6)$$

330 where  $dV/dP$  is known as the pulmonary compliance - a measure of how easy it is  
331 to inflate, which can be obtained by analysing the pressure-volume curve of the lung.  
332 Low compliance indicates a stiff lung and means extra work is required to bring in  
333 a normal volume of air. This occurs as the lungs in this case become fibrotic, lose  
334 their dispensability and become stiffer. On the other hand, patients with a high lung  
335 compliance due to the poor elastic recoil have no problem inflating the lung but have  
336 difficulty exhaling air (Galetke et al., 2007). Combining Eqs.(4) and (6), we have

$$\frac{dP}{E} = -\frac{1}{3(1-2\nu)} \frac{dV}{V_0} \quad (7)$$

337 where the initial lung volume,  $V_0$ , and its volume change,  $dP$ , can be obtained from  
338 4D CT segmentation summarised in Table 1. However, Eq. (7) is only valid for a free  
339 expansion of the lungs under a uniform pressure, which may underestimate the mini-  
340 mum required pleural pressure (Werner et al., 2009a). Because of the effect of contact  
341 interaction between the deformable lung and the rib cage, the minimum required value  
342 of pleural pressure could be much higher. As can be observed in Table 1, Case 6 has the  
343 maximum volume change ratio of 0.3, thus the minimum pleural pressure estimated from  
344 Eq.(7) is 0.83 kPa. If we define the success criteria for FE simulations as the volume of  
345 the deformed lung is  $\geq 99.5\%$  of its final target volume, then this value is too small for  
346 FE simulations. In this study, we found a pressure load of 3 kPa was large enough to  
347 deform a lung to 99.5% of its target volume in FE simulations for all 10 cases. All sim-  
348 ulations were performed with a nonlinear implicit procedure available in the commercial  
349 nonlinear implicit FE solver, ABAQUS/standard, with geometrical nonlinearity included  
350 for large deformation analyses.

351 *2.4. Intensity-based non-rigid image registration*

352 In principle, any non-rigid image registration can be integrated into the proposed reg-  
353 istration scheme. Many different transformation models are available and we refer inter-  
354 ested readers to extensive reviews on medical image registration (Maintz and Viergever,  
355 1998; Holden, 2008; Sotiras et al., 2013) for further information. The choice of registra-  
356 tion method depends on anatomic structures of interest, as well as clinical applications  
357 and constraints. In this study, we attempt to make full use of intensity information in  
358 medical images to provide an accurate registration for internal structures and features.  
359 Therefore, we chose to focus on intensity-based, non-rigid registration schemes, imple-  
360 mented using popular B-spline transformation models (Rueckert et al., 1999; Klein et al.,  
361 2010) (see details in Section 3).

362 *2.5. Evaluation of the proposed algorithm*

363 Dynamic lung images in particular have been used widely for evaluating deformable  
364 image registration algorithms. To evaluate the proposed method and facilitate the com-  
365 parison with other registration methods in the literature, we performed intra-patient  
366 non-rigid registration of 3D CT data drawn from lung cancer patient 4D CT datasets in  
367 the DIR-Lab database ([www.dir-lab.com](http://www.dir-lab.com))(Castillo et al., 2010). These datasets have  
368 already been used for validating and evaluating different registration methods of slid-  
369 ing objects in several publications (Schmidt-Richberg et al., 2012b; Delmon et al., 2013;  
370 Heinrich et al., 2013; Fuerst et al., 2015). In these datasets, each 4D CT scan includes  
371 ten 3D CT images obtained over a breathing cycle. The slice thickness of each 3D CT  
372 image is  $2.5mm$  and the in-plane spatial resolution ranges from  $0.97mm \times 0.97mm$  to  
373  $1.16mm \times 1.16mm$ . Each 3D CT scan comes with a set of 300 inner-lung landmarks,  
374 carefully annotated by experts. Thus, a total of 3000 internal landmarks are available.  
375 The intraobserver variants of the 10 cases range from  $0.70(0.99)mm$  to  $1.13(1.27)mm$ ,  
376 with an average of  $0.88(1.3)mm$ . The uncertainty in the landmark selection is within  
377 the voxel size of the images. The lung volumes of the 10 patients estimated from the  
378 lung segmentation process described in Section 2.3 are listed in Table 1. These values  
379 indicate that the volumes and the expansion rates of lungs during a full breathing cycle  
380 vary significantly between individuals, from 5.5% to 30% (Note also that the left lung is  
381 slightly smaller than the right lung in each case).

382 In this study, we used image pairs consisting of 3D CT images of lungs at the end  
383 of inspiration and their corresponding images at the end of expiration to evaluate the  
384 registration accuracy, in terms of an anatomical-landmark-based target registration error  
385 (TRE). We particularly analysed the registration error distributions of those landmarks  
386 within an inner region of  $10mm$  near lung surfaces, where the accuracy of intensity-based  
387 image registration methods is mostly affected by sliding motion. The effects of parameters  
388 in biomechanical models on displacement estimation have also been investigated.

### 389 **3. Results**

390 To quantify the registration accuracy of the proposed method and investigate the  
391 effects of model parameters, we calculated the target registration error (TRE) defined  
392 as the Euclidean distance between 300 pairs of internal anatomical landmarks which are  
393 provided with the DIR-lab dataset and identified in the target image and transformed  
394 source image space for each case. Furthermore, we compared the proposed method,  
395 referred here to as **FE+B-spline**, with a biomechanical simulation method, a conven-  
396 tional non-rigid B-spline registration without a consideration of sliding motion (Klein  
397 et al., 2010), and two alternative non-rigid intensity-based image registration methods  
398 with a specific handling of sliding motion.

399 The four methods used for the purposes of comparison are summarised as follows

- 400 • **Method 1:** Biomechanical simulation (Werner et al., 2009a,b), (identical to that  
401 used in the first process of the proposed method).
- 402 • **Method 2:** Separate image registration of the lungs and other anatomy using  
403 conventional B-spline registration and lung masks (Wu et al., 2008).
- 404 • **Method 3:** Image registration with sliding regularisation based on direction-  
405 dependent B-spline decompositions (Vandemeulebroucke et al., 2012; Delmon et al.,  
406 2013).
- 407 • **Method 4:** Conventional B-spline registration without special considerations for  
408 sliding motion (Klein et al., 2010).



409 Since the Elastix toolbox for intensity-based image registration (Klein et al., 2010)  
 410 (<http://elastix.isi.uu.nl>), has implemented conventional B-spline transformation  
 411 models being used for Method 2 and Method 4, and sliding motion regularisation scheme  
 412 used in Method 3, it was used in this study. To ensure a fair comparison, the same  
 413 B-spline transformation models and parameters were chosen whenever B-spline registra-  
 414 tion was used. The following settings were used for the B-spline registration algorithm,  
 415 described in (Delmon et al., 2013): (1) Third order B-spline transformations were op-  
 416 timised with up to 16000 iterations using the adaptive stochastic gradient descent to  
 417 guarantee convergence; (2) The spacing between B-spline control points was  $32mm$  in  
 418 each direction (which is large enough to impose spatially smooth deformations without  
 419 additional regularization); (3) The Mattes mutual information metric was used, and the  
 420 moving image was interpolated using third order B-spline; and (4) A multi-resolution  
 strategy with a Gaussian smoothing kernel and three resolution levels was used.

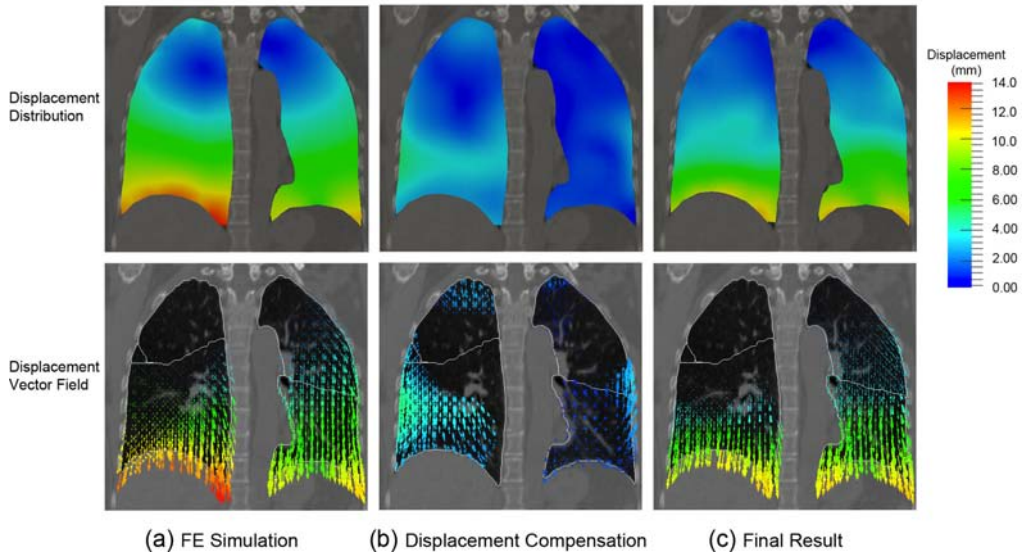


**Figure 3:** Displacement field estimation for Case 1 from two consecutive processes of the proposed method during registration: (a) FE estimated displacement field (b) displacement compensation from the subsequent B-spline registration (c) final displacement field. In the FE simulations, the lungs were assumed to be homogeneous and frictionless against the chest wall. The displacement magnitude ranges from  $0.28mm$  to  $13.6mm$ .

421

422 *3.1. Displacement evolution during registration*

423 Figure 3 illustrates a typical example of displacement evolution during the two-process  
424 registration of our method. The deformed lung models are overlaid on the original CT  
425 image at full inspiration. Both the displacement magnitudes and the directions are plot-  
426 ted. Fig. 3(a) shows a 2D displacement distribution from biomechanical modelling in  
427 the coronal plane for Case 1. In the biomechanical simulations, we assumed that the  
428 two lungs were homogeneous and the interaction between the lungs and the chest wall  
429 was frictionless. Fig. 3(b) is the displacement compensation to biomechanical modelling  
430 by the subsequent non-rigid B-spline registration process, and Fig. 3(c) is the total dis-  
431 placement distribution after the two-process registration. As can be seen in Fig. 3(a),  
432 the FE model captures a substantial part of the lung deformation, and the subsequent  
433 B-spline registration compensates for relatively small residuals ( $< 5.0mm$ ) distributed in  
434 the right lower lobe (Fig. 3(b)).

435 *3.2. Influence of material parameters*

436 To investigate the effect of Poisson’s ratio, we used Case 1 as an exemplar and plotted  
437 the volume ratio between the deformed volume and its target volume against the applied  
438 dimensionless pleural pressure, represented as,  $dP/dE$ , for different values of Poisson’s  
439 ratio  $\nu = (0.1, 0.2, 0.3, 0.4 \text{ and } 0.45)$  (see Fig. 4). Inspection of Fig. 4 reveals that the  
440 higher the value of Poisson’s ratio, the higher the pleural pressure required to deform  
441 the initial lung volume to its target volume. When different values of Poisson’s ratio are  
442 assigned, the volume change follows different paths before finally reaching a plateau close  
443 to 1.0. Therefore, we may conclude that the choice for the value of Poisson’s ratio does  
444 affect biomechanical modelling process of lung motion.

445 In addition, we investigated the effect of Poisson’s ratio on the final deformation field  
446 following a successful FE simulation, that is, when the plateau shown in Fig. 4 is reached.  
447 Figure 5 illustrates the displacement distributions during the registration processes for  
448 different values of Poisson’s ratio. Both FE simulation results and final registration  
449 results using the proposed method are presented. The pattern of the final displacement  
450 fields does not show significant difference between the four FE models with different  
451 values of Poisson’s ratio. After FE simulations, the mean (the standard deviation (SD))  
452 of the target registration errors (TRE) of 300 lung landmarks for the four FE models were

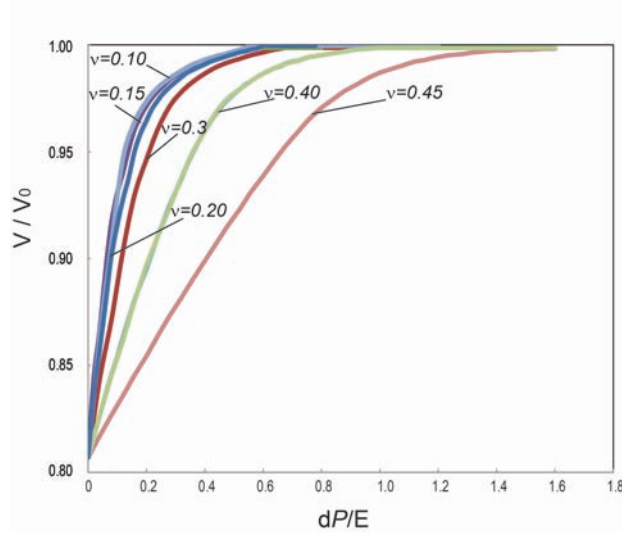


**Figure 4:** Relationships between the increase of pleural pressure and the ratio of the deformed lung volume to its target volume for different values of Poisson's ratio of lung tissues.

453 1.80(0.95)*mm*, 1.79(0.99)*mm*, 1.77(0.92)*mm*, 1.81(1.13)*mm*, respectively. After final  
 454 registration using the proposed method, the final mean (SD) of the TRE was reduced to  
 455 1.06(0.54)*mm*, 1.08(0.54)*mm*, 1.08(0.55)*mm* and 1.09(0.54)*mm*, respectively. Therefore,  
 456 in terms of TREs of landmarks, the choice of Poisson's ratio does not have an obvious  
 457 impact on either the final FE simulation results after the lungs are expanded above 99.5%  
 458 of their target volumes or on the final registration results.

### 459 3.3. Effect of friction

460 For a normal lung, it is expected that the lung and the pleural cavity slide against  
 461 each other smoothly. However, there may exist small friction on the sliding interface due  
 462 to the existence of lung diseases or tumours near lung surfaces. To investigate the fric-  
 463 tion effect on FE simulations and final registration accuracy, a frictional contact model is  
 464 used for patient-specific biomechanical modelling. We used a default setting of ABAQUS  
 465 with a penalty friction formulation for contact analysis, and chose four different values  
 466  $\alpha = (0.05, 0.1, 0.2 \text{ and } 0.3)$  for the friction coefficient,  $\alpha$ . For the sake of simplicity,  
 467 the same parameters were used for both the left and the right lung models. The effect  
 468 of friction on displacement distributions during the proposed registration processes was

469 analysed. Figure 6 shows a comparison of displacement distributions during the registra-  
470 tion processes between a frictionless model and four frictional models. The displacements  
471 obtained from FE simulations, the displacement compensations of B-spline registration,  
472 and the combined results are presented as well.

473 As shown in Fig. 6 (first row), FE simulation results of displacement distribution  
474 are different when different friction coefficients are used in FE models. The pattern  
475 of displacement distributions shows that the motion of the upper lobes of the lungs is  
476 reduced with the increase in the coefficient of friction. The mean (SD) TREs of 300  
477 landmarks are also affected:  $1.77(0.99)mm$  for frictionless case,  $1.67(0.71)mm$  for  $\alpha =$   
478  $0.05$ ,  $1.42(0.67)mm$  for  $\alpha = 0.1$ ,  $1.49(0.77)mm$  for  $\alpha = 0.2$  and  $2.18(1.14)mm$  for  $\alpha =$   
479  $0.3$ , respectively. The FE model with a friction coefficient of 0.1 gives the best prediction  
480 on the displacements of the landmarks, although other choices on friction coefficient  
481 below  $\alpha = 0.3$  produce similar accuracies. The final registration results are presented  
482 on the third row of Fig. 6. The distribution of total displacements shows no difference  
483 when different frictional models are used, this is further confirmed by very small TRE  
484 differences of the landmarks with the combined method. The mean (SD) TREs of the  
485 300 landmarks are  $1.08(0.5)mm$  (frictionless),  $1.05(0.55)mm$  ( $\alpha = 0.05$ ),  $1.04(0.54)mm$   
486 ( $\alpha = 0.1$ ),  $1.06(0.53)mm$  ( $\alpha = 0.2$ ) and  $1.07(0.54)mm$  ( $\alpha = 0.3$ ), respectively.

487 Although FE models with different friction coefficient values produce different dis-  
488 placement estimations, the proposed registration method provides the same registration  
489 accuracy for all models, thanks to the displacement compensation to FE simulations  
490 in the subsequent intensity-based registration. The displacement compensations to FE  
491 models are plotted on the second row of Fig. 6. The larger displacement compensations  
492 to the FE simulations on the right lower lobes close to the chest wall indicate that the  
493 frictionless model may overestimate the displacement of right lower lobes. By introduc-  
494 ing a frictional contact model to limit the motion of the lower lobe near to the chest  
495 wall, the overestimated displacement could be partially compensated. For instance, the  
496 mean TRE was reduced from  $1.77mm$  to  $1.42mm$  by introducing a small amount of fric-  
497 tion (e.g.  $\alpha = 0.1$ , Fig. 6(c)). However, introducing too much friction (e.g.  $\alpha = 0.3$ ,  
498 Fig. 6(d)) may significantly over-constrain the deformation of the upper lobes, causing an  
499 underestimation of the amount of deformation.

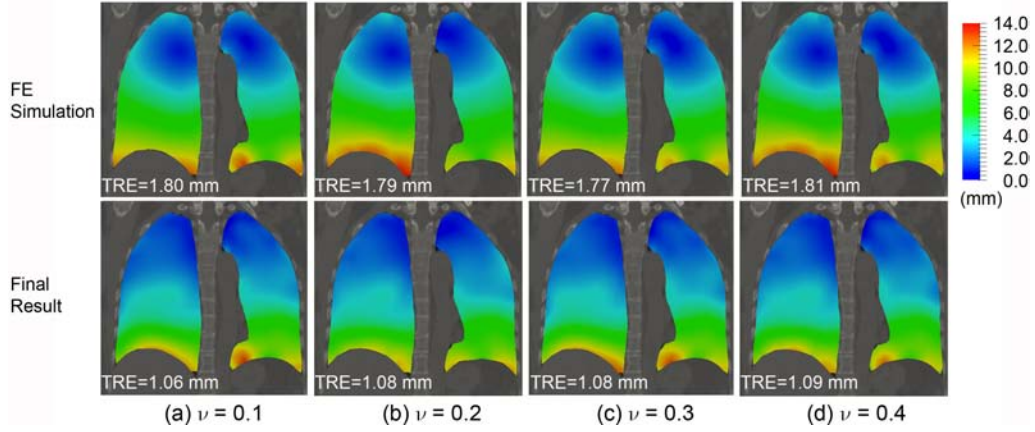


**Figure 5:** Displacement field distributions of the lungs from FE simulations using four different values of Poisson's ratio after the lung models are expanded to their target. The first row shows FE simulation results; the second row shows final registration results using the proposed method. The colour denotes the displacement magnitude increasing from blue to red.

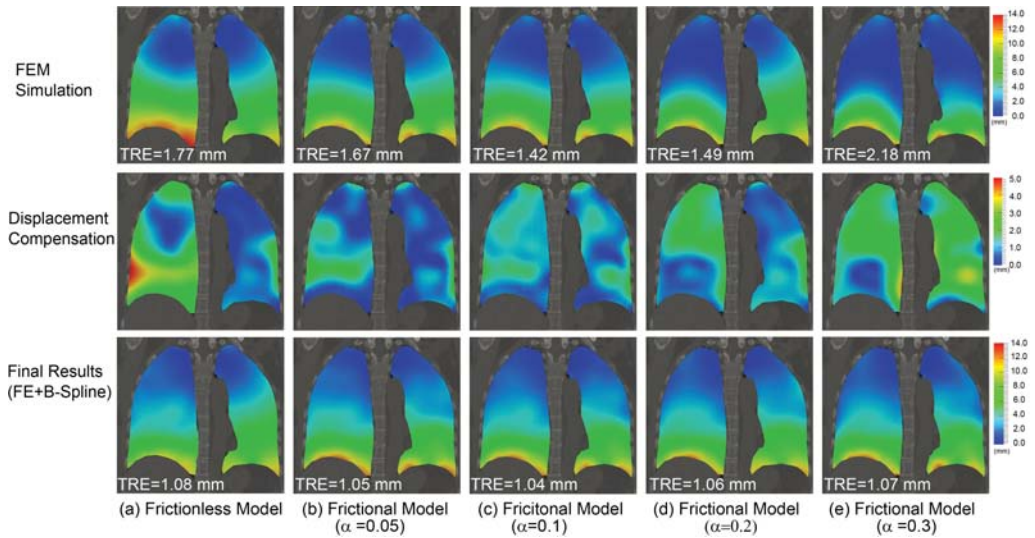


**Figure 6:** Friction effect on finite element simulation results of displacement distribution and final registration accuracy for Case 1. The distributions of displacement magnitude are superimposed on the 2D coronal slice of CT images at full inspiration. The results of a frictionless FE model (a) are compared with those of frictional FE models with different values of friction coefficient (b) 0.05, (c) 0.1 (d) 0.2 and (e) 0.3 . The colour denotes the displacement magnitude increasing from blue to red.

500 *3.4. Effect of tissue heterogeneity*

501 In reality, the tissue distributions of lungs are not homogeneous, but utilising a het-  
502 erogeneous tissue model can significantly increase the complexity of modelling. To in-  
503 vestigate the effect of tissue homogeneity assumption on FE simulations and registration  
504 accuracy, we performed an experiment on Case 8, which has the highest mean TRE er-  
505 ror of  $15mm$  for 300 landmarks among all 10 datasets before registration, as shown in  
506 Table 2.

507 3D CT images of Case 8 revealed a small tumour in the left upper lobe, as shown  
508 in the coronal slice on the second column of Fig. 7, which might severely increase the  
509 stiffness in this region and in turn affects the deformation characteristics. Therefore, we  
510 proposed a heterogeneous FE model to account for the difference in stiffness for each lobe.  
511 The lobes of both lungs were segmented manually using the same process described in  
512 (Han et al., 2014b) and different Young’s moduli were assigned to different lobes. For the  
513 purposes of testing, we assumed that the right lower lobe was softer than both the right  
514 middle and right upper lobes, whilst the left upper lobe was harder than the left lower  
515 lobe due to the existence of a tumour. In the FE model, the right lower lobe was assigned  
516 with a Young’s modulus of 2.5 kPa; the left upper lobe was assigned with a larger value of  
517 Young’s modulus, 10 kPa; and all the other lobes were assigned with a Young’s modulus  
518 of 5 kPa. The choice of Young’s moduli for soft/hard lobes was arbitrary and only for  
519 the purpose of demonstrating the effect of tissue heterogeneity.

520 Figure 7 shows the change in displacement distribution during registration when a  
521 homogeneous tissue model is replaced by a heterogeneous tissue model in the biomechan-  
522 ical modelling process. Frictionless contact is assumed for both models. The distribution  
523 of displacement compensation (the second column in Fig. 7) shows that the homogeneous  
524 tissue model may underestimate the deformations of both the left upper lobe and the  
525 right lower lobe. This may be caused by the difference of each lobe in mechanical prop-  
526 erties or the non-uniform pleural pressure between different lobes (Permutt et al., 1962;  
527 West et al., 1964). In particular, the 3D CT images of Case 8 revealed a small tumour in  
528 the left upper lobe (coronal slice on the second column of Fig. 7), which might severely  
529 increase the stiffness in this region and in turn affects the deformation characteristics.  
530 Therefore, we proposed a heterogeneous FE model to account for the difference in stiff-

531 ness for each lobe. The lobes of both lungs were segmented manually using the same  
532 process described in (Han et al., 2014b) and different Young’s moduli were assigned to  
533 different lobes. Figure 7(b) shows the result of displacement distribution when an FE  
534 model with a heterogeneous distribution of tissues is used. For the purposes of testing,  
535 we assumed that the right lower lobe was softer than both the right middle and right  
536 upper lobes, whilst the left upper lobe was harder than the left lower lobe due to the  
537 existence of a tumour. In the FE model, the right lower lobe was assigned with a Young’s  
538 modulus of 2.5 kPa; the left upper lobe was assigned with a larger value of Young’s mod-  
539 ulus, 10 kPa; and all the other lobes were assigned with a Young’s modulus of 5 kPa.  
540 The choice of Young’s moduli for soft/hard lobes was arbitrary and only for the purpose  
541 of demonstrating the effect of tissue heterogeneity. As shown in Fig. 7, the amount of  
542 displacement compensation from intensity-based registration is much smaller when the  
543 heterogeneous model is used. When the homogeneous model is replaced with the het-  
544 erogeneous model, the mean (SD) TRE of 300 landmarks is reduced from 6.95(3.61)*mm*  
545 to 4.41(2.22)*mm* after FE simulations, showing an improvement in prediction accuracy  
546 of FE modelling on lung motion. However, the final displacement distribution after the  
547 displacement compensation from intensity-based registration does not show visually ob-  
548 vious difference, and the proposed method gave the same registration accuracy, with a  
549 mean (SD) TRE of 1.48(1.05)*mm* for the homogeneous model versus 1.48(1.10)*mm* for  
550 the heterogeneous model, respectively.

551 Since biomechanical models can explicitly include physical properties (such as stiff-  
552 ness) of tumours and characterise their motion behaviour during respiration, it is ex-  
553 pected that introducing the tissue heterogeneity in the biomechanical modelling process  
554 could improve the performance of the hybrid registration method on physically realistic  
555 deformation/motion estimation of tumours. For example, there exists a tumour located  
556 in the lower lobe of the Patient’s left lung in Case 6, as shown in Fig. 8(a). The vol-  
557 ume of the tumour does not show an observable change on 4D CT images. Therefore,  
558 in the FE model, we assume that the tumour has a Young’s modulus of 25 kPa, five  
559 times stiffer than its surrounding tissues. In such a way, we expect that the final volume  
560 change of the tumour in the proposed registration method is small. Our method was  
561 compared with two non-rigid B-spline registrations with a specific consideration of sliding

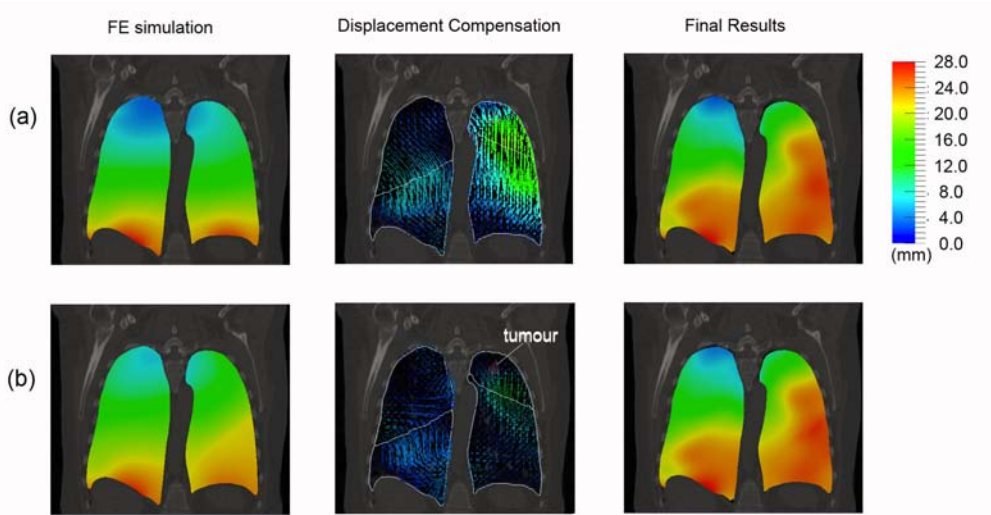


**Figure 7:** A comparison of displacement distributions during the two-process registration between (a) a homogeneous model and (b) a heterogeneous model.

562 motion: Method 2 (Wu et al., 2008) and Method 3 (Delmon et al., 2013), outlined above.  
563 Figure 8 presents the maps of estimated lung volume changes with the three methods  
564 for Case 6. It shows that the two intensity-based B-spline transformations fail to pre-  
565 serve the volume of the tumour, although all three methods produce the same pattern  
566 of volume change and the similar registration errors for Case 6. Another non-rigid image  
567 registration method that can cope with the sliding motion, MRF-based deformable  
568 registration (Heinrich et al., 2013), also did not provide sufficient volume preservation  
569 of the tumour for Case 6 (see Fig.3 in the reference (Heinrich et al., 2013)). **Although**  
570 **the volume preservation can also be kept under the framework of intensity-based image**  
571 **registration methods, e.g. with a tissue-dependent filtering method (Staring et al., 2007)**  
572 , it is much easier for our method to preserve the tumour volume by directly including  
573 tumour-specific physical data, such as stiffness which may be measured from elasticity  
574 imaging/biopsy, into biomechanical models. The results demonstrates that the proposed  
575 registration method has an advantage in volume preservation relevant to the scenario  
576 where a hard tumour exists,



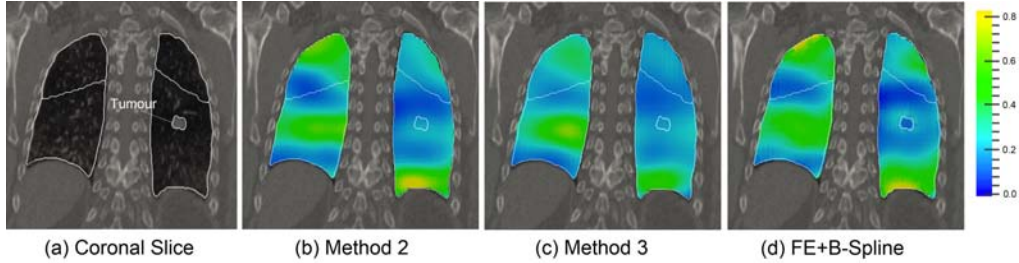


**Figure 8:** A comparison of volume change ratio for Case 6 with three methods: (b) Method 2, Separate image registration based on B-splie and lung masks (c) Method 3: B-spline image registration with sliding regularisation and (d) our method (FE+B-spline). Fig. 8(a) is a 2D coronal slice superimposed with a contour of a hard tumour and the contours of lung lobes. Although all of the three methods produce the same pattern of volume increase, our method can explicitly include the stiffness information of the tumour to ensure volume preservation.

### 577 3.5. Quantitative comparison and evaluation

578 As stated above, the proposed algorithm was evaluated quantitatively by calculating  
 579 the TREs for 300 internal lung landmarks for each case. Our method, FE+B-spline,  
 580 was compared with four methods, Methods 1-4 outlined above. Table 2 summarises the  
 581 mean(SD) TREs over 300 landmarks for each lung cancer patient and for each of the  
 582 five registration methods. The results show that biomechanical modelling (Method 1),  
 583 could achieve better registration accuracy (mean TRE= 3.81mm) than Method 4 (mean  
 584 TRE= 4.57mm), even if a simple homogeneous FE model is used. Our method has  
 585 achieved a registration accuracy comparable to Method 2 and Method 3, both of them  
 586 consider the effect of sliding motion.

587 To compare the five registration methods in terms of registration error distribution, we  
 588 calculated both accumulated and frequency distributions of TRE for all 3000 landmarks  
 589 of 10 cases (300 landmarks per patient) for each method. In addition, we evaluated  
 590 the registration error distribution, using the landmarks near the surface of the lungs  
 591 where sliding occurs, defined as the landmarks lying within an inner region of 10 mm  
 592 near the surface. Accurate registration on surface regions is particularly important for  
 593 the accurate dose **accumulation** in the radiotherapy and HIFU (high intensity focused  
 594 ultrasound) ablation of tumours, such as non-small cell lung cancer, adenocarcinoma,  
 595 large cell carcinoma, and pleural mesothelioma covering on the lung surface (Muers,

**Table 2:** Registration Results of Five Registration Methods (Mean TRE(SD) in *mm*). The five methods are Method 1: Biomechanical simulation; Method 2: Separate image registration based on B-spline and lung masks; Method 3: B-spline image registration with sliding regularisation; Method 4: Conventional B-spline registration; and Our Method (FE+B-Spline), respectively. The calculation of mean TRE(SD) uses all 300 landmarks for each subject.

Patient	Before Registration	Method 1	Method 2	Method 3	Method 4	Our Method (FE+B-Spline)
1	3.89(2.78)	1.77(0.92)	1.14(0.64)	1.21(0.52)	1.63(1.09)	1.08(0.55)
2	4.34(3.90)	2.14(1.28)	1.03(0.50)	1.06(0.52)	1.85(1.88)	0.99(0.49)
3	6.94(4.05)	3.90(2.10)	1.28(0.67)	1.83(1.02)	3.26(2.47)	1.22(0.65)
4	9.83(4.85)	4.04(2.21)	1.50(1.01)	1.71(1.09)	3.34(2.85)	1.49(0.99)
5	7.48(5.50)	3.39(2.17)	1.88(1.41)	1.94(1.54)	4.18(3.80)	1.73(1.38)
6	10.9(6.96)	3.54(2.23)	1.52(0.87)	1.70(0.94)	5.10(4.46)	1.48(0.86)
7	11.0(7.42)	4.22(2.91)	1.61(1.09)	1.98(1.30)	7.07(6.42)	1.50(0.85)
8	15.0(9.00)	6.95(3.61)	1.49(1.13)	2.41(2.45)	10.88(9.63)	1.48(1.05)
9	7.9(3.97)	4.26(1.91)	1.40(0.76)	1.56(0.86)	4.32(2.94)	1.38(0.71)
10	7.3(6.34)	3.89(2.46)	1.51(1.08)	1.71(1.22)	4.07(4.66)	1.41(0.84)
Mean(SD)	8.46(5.62)	3.81(2.65)	1.45(0.99)	1.71(1.31)	4.57(5.32)	1.37(0.89)

596 2003). Of the 3000 internal landmarks available, 554 were located in the near-surface  
 597 region. The corresponding registration results are presented in Figs. 9.

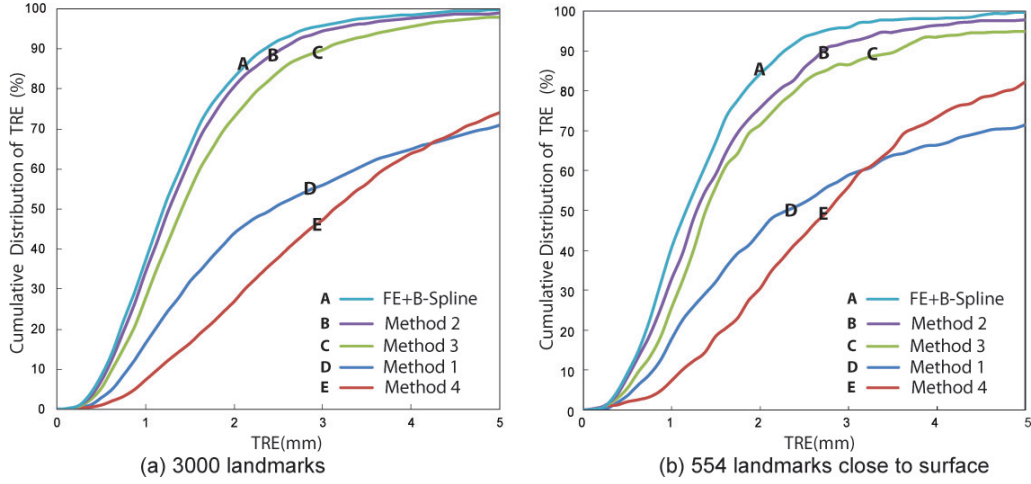


**Figure 9:** Cumulative distributions of the TRE of landmarks for 10 subjects (Case1-Case10): (a) all of 3000 landmarks (2) 554 landmarks near the lung surface within a  $10mm$  depth. Five registration methods are compared, including (A) Our method, FE+B-spline; (B) Method 2, Separate image registration based on B-spline and lung masks; (C) Method 3, B-spline with sliding regularisation; (D) Method 4, Conventional B-spline; and (E) Method 1, Biomechanical simulation.

598 As shown in Fig. 9, our method produces the lowest registration error in terms of cu-  
 599 mulative distributions of the TREs. When all the landmarks are taken into account,  
 600 numerically, the proposed method is superior to Method 3 and slightly better than  
 601 Method 2. The mean (SD) TREs of Methods 1-5 are  $3.81(2.65)mm$ ,  $1.45(0.99)mm$ ,  
 602  $1.71(1.31)mm$ ,  $4.57(5.32)mm$  and  $1.37(0.89)mm$ , as listed in Table 2.

603 When only the landmarks near the lung surface are considered, our method also per-  
 604 forms better than any other methods(see Fig.9(b)). The mean (SD) TREs with the five  
 605 registration methods are  $3.35(2.4)mm$ ,  $1.60(2.14)mm$ ,  $1.96(1.35)mm$ ,  $4.9(6.21)mm$  and  
 606  $1.33(0.79)mm$ , respectively. The maximum errors corresponding to the five methods are  
 607  $20.7mm$ ,  $19.1mm$ ,  $15.7mm$ ,  $24.9mm$  and  $5.3mm$ , respectively. The number of landmarks  
 608 with a  $TRE > 5mm$  is 98, 8, 28, 86 and 2 for the four methods, respectively. These re-  
 609 sults suggest that the proposed method provides a better registration accuracy on the  
 610 near-surface regions in terms of the landmarks.

## 611 4. Discussion

### 612 4.1. Registration accuracy

613 Compared to intensity-based image registration methods, biomechanical models for  
614 4D CT lung motion estimation can explicitly model certain breathing dynamics and pro-  
615 vide physically realistic results. However its registration accuracy in terms of landmark  
616 errors is overshadowed by intensity-based image registration methods due to a lack of  
617 considering the anatomic details. To improve the registration performance and best pre-  
618 serve the desired properties of biomechanical modelling, we introduced an intensity-based  
619 image registration process to compensate the displacement residuals of biomechanical  
620 modelling. The results presented in Section 3 show that the proposed method can sig-  
621 nificantly reduce the overall TRE, the mean TRE of the 10 cases drops from 3.81 mm to  
622 1.37mm.

623 The accuracy of the proposed approach compared well with results of previously pub-  
624 lished methods on the same datasets, for example, our method (mean TRE= 1.37mm);  
625 non-rigid diffusion registration with direction-dependent regularization for sliding mo-  
626 tion (Schmidt-Richberg et al., 2012b) (mean TRE=2.13mm, improved to 1.55mm in  
627 (Schmidt-Richberg et al., 2012a)); B-spline registration with direction dependent B-  
628 splines decomposition for sliding motion (mean TRE=1.71mm (Delmon et al., 2013))  
629 and Markov random field (MRF)-based deformable registration (mean TRE=1.52mm,  
630 and 1.43mm with a hyper-label for intensity correction and measurement of the density  
631 change (Heinrich et al., 2013)). Particularly we evaluated the registration performance  
632 of our method on the near-surface regions where the accuracy of intensity-based image  
633 registration methods often suffers from the difficulty in handling with the sliding motion  
634 of lungs against rib cage and diaphragm. We compared our method with a conventional  
635 B-spline based image registration method without a regularisation on sliding motion, and  
636 two B-spline based image registration methods with a specific consideration of sliding  
637 motion. It was found that our method provided better registration performance, which  
638 may be due to explicitly modelling of lung sliding with FE models.. The performance  
639 improvement may be especially important for the cases when there is a need for an  
640 accuracy localization of mobile, superficial tumour, e.g. in radiotherapy applications.

641 Although our methods performed the best in the accuracy evaluation of algorithms

642 on the 4D CT datasets of 10 lung cancer patients publicly available, we do not expect  
643 that the combined approach would definitely result in better results than other recently  
644 developed intensity-based image registration algorithms with a specific consideration of  
645 sliding motion. Rather, we feel that the combination of both approaches facilitates the  
646 handling of **various physical and physiological properties** modelling through an integrated  
647 biomechanical model, helps to improve the registration accuracy near the surface regions,  
648 and potentially provides a guide for improving predictive biomechanical models through  
649 analysing the pattern of displacement compensation from the intensity-based image reg-  
650 istration process.

#### 651 *4.2. Biomechanical model and parameters*

652 In the proposed method, a nonlinear hyperelastic material model was chosen for  
653 biomechanical modelling due to large deformation of the lungs. Previous studies (Al-  
654 Mayah et al., 2009; Werner et al., 2009a) showed that a hyper-elastic material model  
655 produced slightly better prediction results on displacement than a linear model, but the  
656 difference between the two models was small if a contact model was included to simulate  
657 the pleural sliding. In this study, we found that the change of Poisson’s ratio did not  
658 show a significant impact on the displacement distribution of FE models after the lung  
659 was expanded to more than 99.5% of its target volume, but it did affect the deformation  
660 states of lungs during the loading process. As shown in Fig. 4, the volume change of  
661 lungs follows different paths with increasing loading for different values of Poisson’s ratio.  
662 Therefore, it is critical to choose an optimal value for the Poisson’s ratio if biomechanical  
663 models are used for the purpose of predicting the motion in all phases of the respiratory  
664 cycle rather than only finding the absolute difference in deformation between two phases.

665 Like most of studies of lung motion with biomechanical modelling, we only consid-  
666 ered the sliding motion between the entire lung and the chest wall, and ignored the  
667 intra-lobar sliding. This treatment was based on the consideration that the significance  
668 of intralobar sliding in the FE model may be limited during free breathing 4D CT imag-  
669 ing. Amelons PhD study (Amelon, 2012) indicated that the registration accuracy of FE  
670 simulations, based on 4D CT lung images, was not improved after introducing frictionless  
671 lobar sliding. Moreover, the lobar segmentations on 4D CT images are difficult due to  
672 unclear/incomplete fissures on images. To our best knowledge, an automatic lobar seg-

673 mentation of 4D CT lung images does not exist, and the lung lobar segmentation has to  
674 be performed manually. Different interpretation of fissure location may have a more sig-  
675 nificant impact on the FE solution than considering lobar sliding itself in the FE model.  
676 However, lobar sliding may need to be explicitly modelled if volume changes of lungs  
677 are large, e.g. during a breath-hold CT scanning, or understanding the regional lung  
678 function is important (Amelon et al., 2014). In contrast to the difficulty of lobar segmen-  
679 tation, the segmentation of entire lungs are relatively easier. In this study, we adopted  
680 a semi-automatic method. It is understandable that the segmentation inconsistency will  
681 affect the accuracy of FE simulations, but its impact is not significant considering that  
682 the volume change of an FE model due to segmentation inconsistency is small, com-  
683 pared with the entire volume of a lung. However, the segmentation inconsistency may  
684 result in inaccuracy along the boundary of the lungs in image registration, since the  
685 image intensity-based cost function will drive the boundaries of the lung segmentations  
686 obtained from the two images to match (Wu et al., 2008).

687 In the hybrid method, biomechanical models facilitate the simulations of lung’s inter-  
688 actions with the chest wall, which is a big challenge for intensity-based non-rigid image  
689 registration methods. For example, during respiratory, pleural integrity and pleural fluid  
690 provide a very low friction between the lungs and the chest wall, thus, a frictionless  
691 contact may be sufficient to model the sliding motion, as we did in this study. If the  
692 lubrication condition in the pleural cavity changes due to a lung disease, such as pleural  
693 adhesion or pleural effusion, a frictional contact could be defined for the contact pairs  
694 of the FE model to model the lung sliding and investigate the disease-induced change of  
695 lung sliding motion. As shown in Fig. 6, the effect of different friction conditions on lung  
696 deformation could be simulated through adjusting friction coefficients. If a more seri-  
697 ous lung disease occurs, such as pleural invasion by peripheral lung cancer or chest wall  
698 invasion (Sakuma et al., 2017), local lung sliding motion can be completely restricted,  
699 often requiring surgical correction. In such a case, the cohesive interaction behaviour  
700 can be defined for the contact pair between a tumour and the chest wall to model the  
701 attachment of the tumor with the chest wall in the FE model.

702 The results presented in Section 3 show that the accuracy of FE simulations is affected  
703 by model parameters, such as Poisson’s ratio, friction coefficient and tissue heterogeneity,

704 but a simple biomechanical model with a homogeneous frictionless model can provide a  
705 fair good registration results, an average TRE of 3.8 mm, as shown in Table 2. In general,  
706 it is difficult to accurately measure or estimate these parameters. However, the effects of  
707 their uncertainties on image registration accuracy can be reduced in the proposed method  
708 by adding an image registration step to compensate for displacement residuals of an initial  
709 biomechanical simulation using estimated model parameters. With the proposed  
710 method, the changes of these model parameters did not show a significant impact on the  
711 registration accuracy in terms of final TRE. Therefore, introducing this step makes it  
712 possible to reduce the complexity and the computational time of the biomechanical mod-  
713 elling in the first step by employing a simple homogeneous biomechanical model without  
714 compromising the overall registration performance. To further speed up the algorithm,  
715 the parallel implementation of finite element methods on GPU (Han et al., 2014b) could  
716 be adopted. The registration accuracy of the hybrid method can also be improved. Fol-  
717 lowing the method by Zhong et al (Zhong et al., 2012), the estimated displacement fields  
718 from the hybrid method may be used to improve the registration accuracy in low-contrast  
719 regions, where one expects that the deformation estimation is less accurate due to ho-  
720 mogeneous image intensity. More specifically, we can remesh and re-run the FE model  
721 by only applying the displacements estimated from the hybrid method to those nodes of  
722 the FE model lying outside of low-contrast region as displacement boundary conditions,  
723 and recalculate the displacement distributions of these low-contrast regions. Thus, the  
724 execution time and registration accuracy of the hybrid method could be further improved  
725 in the future.

#### 726 4.3. *Potential applicaitons and ongoing work*

727 The hybrid method has provided a comparable registration accuracy as some state-of-  
728 the-art intensity-based image registrations, meanwhile introducing biomechanical models  
729 facilitates various physiological properties modelling of the lungs, such as sliding motion,  
730 heterogeneity of tissue stiffness, friction, pressure difference etc., within one single FE  
731 model, such an integrated solution is unknown for intensity-based image registration  
732 methods. In the proposed method, the biomechanical modelling process in the first step  
733 estimates most of physically realistic deformations of the lungs, and only a relatively  
734 small deformation residual need to be recovered in the intensity-based image registration

735 process of the second step, thus reducing the possibility of creating physically unrealistic  
736 deformation. This advantage of the hybrid method over intensity-based image registra-  
737 tion methods needs to be further investigated and confirmed with phantom tests (Kim  
738 et al., 2016) in which a ground truth can be generated. this is our ongoing work.

739 Since the displacement compensation in the intensity-based image registration pro-  
740 cess reflects the distributions of the prediction errors of biomechanical modelling, it has  
741 a potential to be used for analysing the factors affecting the accuracy of biomechanical  
742 modelling. For example, as indicated in Section 3, based on the analysis of displace-  
743 ment compensation patterns, the simulation accuracy of biomechanical models can be  
744 improved by introducing a small amount of friction for Case 1 or considering the tissue  
745 heterogeneity for Case 8.

746 In the framework of the proposed method, we can also estimate model parameters,  
747 such as friction coefficient, Young’s modulus and Poisson’s ratio, with an optimisation  
748 process through perturbation within realistic reported ranges determined from *in vivo/in*  
749 *vitro* experiments or experience values (Han et al., 2012; Amelon, 2012; Li et al., 2013),  
750 and minimising the required displacement compensation from the intensity-based image  
751 registration process could be an ideal objective function. The estimations of model  
752 parameters can potentially be used for the diagnosis and assessment of lung diseases.  
753 For example, pleural effusion, a condition in which excess fluid accumulated within the  
754 pleural space, and pleural adhesion and pleural invasion by peripheral lung cancer, all  
755 of these diseases can cause the change of lubrication within the pleural cavity locally  
756 or globally. The assessment of lung sliding through assessing the friction of the lung  
757 surfaces can provide aids for physicians in deciding whether a tumour has invaded into  
758 the chest wall, and whether extensive surgery is necessary in the treatment planning  
759 (Sakuma et al., 2017). This application will be further explored.

760 Due to the predictive capacity of biomechanical models, the developed method has  
761 a potential to be used in adaptive radiotherapy. For example, accurate margins for  
762 tumour motion are very important for accurate tumour targeting and sparing healthy  
763 tissues from radiation. However, tumours and healthy tissues may change in shape,  
764 location and stiffness during the course of treatment, which may affect the deformation  
765 and motion of tumours and the lungs. Moreover, patient’s breathing pattern changes



766 from time to time. Therefore, the estimated margin in the treatment planning, based on  
767 non-rigid intensity-based image registration on 4D CT data, may not represent the real  
768 margin for the delivery; there is a risk of missing the target or unnecessary radiation to  
769 normal tissues. Although the motion models based on non-rigid intensity-based image  
770 registration, incorporating with surrogates, are capable of predicting the lung motion over  
771 a complete normal breathing cycle, its prediction capacity on the motion and deformation  
772 of tumours and inner lung tissues is limited, when subjected to breathing irregularity  
773 and the changes of tumours and healthy tissues. However, physics and physiology based  
774 biomechanical models of the lungs can address this limitation. Through assessing the  
775 impacts of these changes on motion and deformation of the tumours and the lungs, a new  
776 modified FE model incorporating these changes can be constructed and used to generate  
777 an FE-estimated motion model. Then, the FE-estimated motion model is refined with  
778 the image registration process of the hybrid method using the FE-estimated CT image  
779 and a treatment CT image (e.g. cone-beam CT) to provide a revised motion model and  
780 tumour trajectory, thus helping radiation oncologists to adjust the radiation treatment  
781 plan in order to prevent insufficient radiation dose to the tumours and excessive radiation  
782 dose to the healthy tissues during the course of treatment.

783 In future work, we plan to investigate extending our method to incorporate informa-  
784 tion on displacement compensation from image registration into an optimisation scheme  
785 for model parameters extraction (e.g. heterogeneous tissue distribution/tissue mechan-  
786 ical properties, friction, non-uniform pleural pressure distribution (Fuerst et al., 2015),  
787 boundary constraints et al), with the aim of determining a more accurate physically re-  
788 alistic biomechanical motion model of the lung and the distribution of stiffness of lung  
789 tissues and pressure distribution which may be directly related with the respiratory func-  
790 tion of lungs (Li et al., 2013; Fuerst et al., 2015).

## 791 5. Conclusion

792 In this paper, we have proposed a hybrid biomechanical-model based image regis-  
793 tration method for lung motion estimation in which sliding motion could be explicitly  
794 modelled. The proposed method consists of two consecutive processes: patient-specific  
795 biomechanical modelling followed by intensity-based image registration. Patient-specific

796 biomechanical modelling simulates biomechanical behaviour of tissues and captures phys-  
797 ically plausible deformation, while image-registration process is used for displacement  
798 compensation to biomechanical modelling by making full use of intensity patterns of  
799 medical images. The proposed method has been evaluated on lung motion estimation. A  
800 quantitative comparison to three representative registration approaches for lung motion  
801 estimation shows that the hybrid method could provide good registration accuracy when  
802 recovering lung deformation, especially in the near-surface regions, which is particularly  
803 relevant to radiotherapy applications involving the treatment of mobile, superficial tu-  
804 mours. The preliminary study on the effect of parameters in biomechanical models to  
805 deformation fields has found that model parameters (Poisson's ratio, friction) and the  
806 tissue heterogeneity affect the accuracy of biomechanical modelling in the first process  
807 of the proposed registration method, although they have no obvious impact on final  
808 registration performance of the proposed method. It has also demonstrated that the  
809 proposed method has the potential in optimising patient-specific biomechanical models  
810 through analysing the pattern of displacement compensation from the image-registration  
811 process, if the purpose of applications is to develop more accurate, predictable, physical  
812 models.

### 813 **Acknowledgements**

814 The authors wish to acknowledge financial support from EPSRC program Grant  
815 EP/F025750/1 and EP/H046410. The work is also sponsored by Shanghai Pujiang Pro-  
816 gramme(16PJ1409400).

- 817 Al-Mayah, A., Moseley, J., Brock, K.K., 2008. Contact surface and material nonlinearity modeling of  
818 human lungs. *Physics in Medicine and Biology* 53, 305–317.
- 819 Al-Mayah, A., Moseley, J., Velec, M., Brock, K.K., 2009. Sliding characteristic and material compress-  
820 ibility of human lung: Parametric study and verification. *Medical Physics* 36, 4625–4633.
- 821 Al-Mayah, A., Moseley, J., Velec, M., Hunter, S., Brock, K., 2010. Deformable image registration of  
822 heterogeneous human lung incorporating the bronchial tree. *Medical Physics* 37, 4560–4571.
- 823 Al-Mayah, A., Moseley, J., Velec, M., Hunter, S., Brock, K., 2011. Toward efficient biomechanical-based  
824 deformable image registration of lungs for image-guided radiotherapy. *Physic in Medicine and Biology*  
825 56, 4701–4513.
- 826 Amelon, R., 2012. Development and charactrization of a finite element model of lung motion. Ph.D.  
827 thesis. University of Iowa.
- 828 Amelon, R., Cao, K., Christensen, G., Raghavan, M.A., 2014. A measure for characterizing sliding on  
829 lung boundaries. 2014;42(3):642-650. *Annals of Biomedical Engineering* 42, 642–650.
- 830 Castillo, E., Castillo, R., Martinez, J., Shenoy, M., Guerrero, T., 2010. Four-dimensional deformable  
831 image registration using trajectory modeling. *Physics in Medicine and Biology* 55, 305–327.
- 832 Castillo, R., Castillo, E., Guerra, R., Johnson, V.E., McPhail, T., Garg, A.K., Guerrero, T., 2009. A  
833 framework for evaluation of deformable image registration spatial accuracy using large landmark point  
834 sets. *Physics in Medicine and Biology* 54, 1849–1870.

- 835 Delmon, V., Rit, S., Pinho, R., Sarrut, D., 2013. Registration of sliding objects using direction dependent  
836 b-splines decomposition. *Physics in Medicine and Biology* 58, 1303–1314.
- 837 Fuerst, B., Mansi, T., Carnis, F., M, S., xe, Izle, Zhang, J., Declerck, J., Boettger, T., Bayouth, J.,  
838 Navab, N., Kamen, A., 2015. Patient-specific biomechanical model for the prediction of lung motion  
839 from 4-d ct images. *IEEE Transactions on Medical Imaging* 34, 599–607.
- 840 Galetke, W., Feier, C., Muth, T., Ruehle, K.H., Borsch-Galetke, E., Randerath, W., 2007. Reference  
841 values for dynamic and static pulmonary compliance in men. *Respiratory Medicine* 101, 1783–1789.
- 842 Gray, H., 1918. *Anatomy of the Human Body*. Lea&Febiger, Philadelphia.
- 843 Han, L., Hawkes, D., Barratt, D., 2014a. A hybrid biomechanical model-based image registration method  
844 for sliding objects, in: *SPIE Medical Imaging*, pp. G1–G6.
- 845 Han, L., Hipwell, J.H., Eiben, B., Barratt, D., Modat, M., Ourselin, S., Hawkes, D.J., 2014b. A nonlinear  
846 biomechanical model based registration method for aligning prone and supine mr breast images. *IEEE*  
847 *Transactions on Medical Imaging* 33, 682–694.
- 848 Han, L., Hipwell, J.H., Tanner, C., Taylor, Z., Mertzaniidou, T., Cardoso, J., Ourselin, S., Hawkes, D.J.,  
849 2012. Development of patient-specific biomechanical models for predicting large breast deformation.  
850 *Physics in Medicine and Biology* 57, 455 – 472.
- 851 Heinrich, H.P., Jenkinson, M., Brady, M., Schnabel, J.A., 2013. Mrf-based deformable registration and  
852 ventilation estimation of lung ct. *IEEE Transactions on Medical Imaging* 32, 1239–1248.
- 853 Heinrich, M., Jenkinson, M., Brady, M., Schnabel, J., 2010. Discontinuity preserving regularisation for  
854 variational optical-flow registration using the modified lp norm, in: *Medical Image Analysis for the*  
855 *Clinic-A Grand Challenge, Workshop MICCAI 2010*.
- 856 Hipwell, J.H., Vavourakis, V., Han, L., Mertzaniidou, T., Eiben, B., Hawkes, D.J., 2016. A review of  
857 biomechanically informed breast image registration. *Physics in Medicine and Biology* 61, R1.
- 858 Holden, M., 2008. A review of geometric transformations for nonrigid body registration. *IEEE Trans-*  
859 *actions on Medical Imaging* 27, 111–128.
- 860 Kim, J., Saitou, K., Matuszak, M.M., Balter, J.M., 2016. A finite element head and neck model as  
861 a supportive tool for deformable image registration. *International Journal of Computer Assisted*  
862 *Radiology and Surgery* 11, 1311–1317.
- 863 Klein, S., Staring, M., Murphy, K., Viergever, M.A., Pluim, J.P.W., 2010. Elastix: A toolbox for  
864 intensity-based medical image registration. *IEEE Transactions on Medical Imaging* 29, 196–205.
- 865 Li, M., Castillo, E., Zheng, X.L., Luo, H.Y., Castillo, R., Wu, Y., Guerrero, T., 2013. Modeling  
866 lung deformation: A combined deformable image registration method with spatially varying young’s  
867 modulus estimates. *Medical Physics Letter* 40, 1–10.
- 868 Li, P., Malsch, U., Bendl, R., 2008. Combination of intensity-based image registration with 3d simulation  
869 in radiation therapy. *Physics in Medicine and Biology* 53, 4621–4637.
- 870 Maintz, J.B.A., Viergever, M.A., 1998. A survey of medical image registration. *Medical Image Analysis*  
871 2, 1–36.
- 872 McClelland, J.R., Blackall, J.M., Tarte, S., Chandler, A.C., Hughes, S., Ahmad, S., Landau, D.B.,  
873 Hawkes, D.J., 2006. A continuous 4d motion model from multiple respiratory cycles for use in lung  
874 radiotherapy. *Medical Physics* 33, 3348–3358.
- 875 McClelland, J.R., Hawkes, D.J., Schaeffter, T., King, A.P., 2013. Respiratory motion models: A review.  
876 *Medical Image Analysis* 17, 19–42.
- 877 Muers, M.F., 2003. Lung cancer. *Medicine* 31, 28–37.
- 878 Murphy, K., Ginneken, B.v., Reinhardt, J.M., Kabus, S., Ding, K., Deng, X., Cao, K., Du, K., Chris-  
879 tensen, G.E., Garcia, V., Vercauteren, T., Ayache, N., Commowick, O., Malandain, G., Glocker, B.,  
880 Paragios, N., Navab, N., Gorbunova, V., Sporring, J., Bruijne, M.d., Han, X., Heinrich, M.P., Schn-  
881 abel, J.A., Jenkinson, M., Lorenz, C., Modat, M., McClelland, J.R., Ourselin, S., Muenzing, S.E.A.,  
882 Viergever, M.A., Nigris, D.D., Collins, D.L., Arbel, T., Peroni, M., Li, R., Sharp, G.C., Schmidt-  
883 Richberg, A., Ehrhardt, J., Werner, R., Smeets, D., Loeckx, D., Song, G., Tustison, N., Avants, B.,  
884 Gee, J.C., Staring, M., Klein, S., Stoel, B.C., Urschler, M., Werlberger, M., Vandemeulebroucke, J.,  
885 Rit, S., Sarrut, D., Pluim, J.P.W., 2011. Evaluation of registration methods on thoracic ct: The  
886 empire10 challenge. *IEEE Transactions on Medical Imaging* 30, 1901–1920.
- 887 O’Rahilly, R., Mller, F., Carpenter, S., Rand Swenson, D., 2004. *Basic Human Anatomy : A Regional*  
888 *Study of Human Structure*. Online version, Dartmouth Medical School.
- 889 Pace, D.F., Enquobahrie, A., Hua, Y., Aylward, S.R., Niethammer, M., 2011. Deformable image reg-  
890 istration of sliding organs using anisotropic diffusive regularization, in: *Biomedical Imaging: From*  
891 *Nano to Macro, 2011 IEEE International Symposium on*, pp. 407–413.
- 892 Permutt, S., Bromberger-Barnea, B., Bane, H., 1962. Alveolar pressure, pulmonary venous pressure,  
893 and the vascular waterfall. *Medical Thoraces* 19, 239–260.

- 894 Rietzel, E., Chen, G.T.Y., 2006. Deformable registration of 4d computed tomography data. *Medical*  
895 *Physics* 33, 4423–4430.
- 896 Risser, L., Vialard, F.X., Baluwala, H.Y., Schnabel, J.A., 2013. Piecewise-diffeomorphic image registra-  
897 tion: Application to the motion estimation between 3d ct lung images with sliding conditions. *Medical*  
898 *Image Analysis* 17, 182–193.
- 899 Ruan, D., Esedoglu, S., Fessler, J.A., 2009. Discriminative sliding preserving regularization in medical  
900 image registration, in: *Biomedical Imaging: From Nano to Macro, 2009. ISBI '09. IEEE International*  
901 *Symposium on*, pp. 430–433.
- 902 Rueckert, D., Sonoda, L.I., Hayes, C., Hill, D.L.G., Leach, M.O., Hawkes, D.J., 1999. Nonrigid registra-  
903 tion using free-form deformations: application to breast mr images. *IEEE Transactions on Medical*  
904 *Imaging* 18, 712–721.
- 905 Sakuma, K., Yamashiro, T., Moriya, H., Murayama, S., Ito, H., 2017. Parietal pleural invasion/adhesion  
906 of subpleural lung cancer: Quantitative 4-dimensional ct analysis using dynamic-ventilatory scanning.  
907 *European Journal of Radiology* 87, 36–44.
- 908 Samavati, N., Velec, M., Brock, K., 2015. A hybrid biomechanical intensity based deformable image  
909 registration of lung 4d ct. *Physics in Medicine and Biology* 60, 3359–3373.
- 910 Schmidt-Richberg, A., Ehrhardt, J., Werner, R., Handels, H., 2012a. Fast explicit diffusion for registra-  
911 tion with direction-dependent regularization, in: Dawant, B., Christensen, G., Fitzpatrick, J.M.,  
912 Rueckert, D. (Eds.), *Biomedical Image Registration. Springer Berlin Heidelberg. volume 7359 of Lec-  
913 ture Notes in Computer Science. book section 23*, pp. 220–228.
- 914 Schmidt-Richberg, A., Werner, R., Handels, H., Ehrhardt, J., 2012b. Estimation of slipping organ motion  
915 by registration with direction-dependent regularization. *Medical Image Analysis* 16, 150–159.
- 916 Sotiras, A., Davatzikos, C., Paragios, N., 2013. Deformable medical image registration: A survey. *IEEE*  
917 *Transactions on Medical Imaging* 32, 1153–1190.
- 918 Staring, M., Klein, S., Pluim, J.P.W., 2007. Nonrigid registration with tissue-dependent filtering of the  
919 deformation field. *Physics in Medicine and Biology* 52, 6879–6892.
- 920 Vandemeulebroucke, J., Bernard, O., Rit, S., Kybic, J., Clarysse, P., Sarrut, D., 2012. Automated  
921 segmentation of a motion mask to preserve sliding motion in deformable registration of thoracic ct.  
922 *Medical Physics* 39, 1006–1015.
- 923 Villard, P., Beuve, M., Shariat, B., Baudet, V., Jaillet, F., 2005. Simulation of lung behaviour with finite  
924 elements: influence of bio-mechanical parameters, in: *Third International Conference on Medical*  
925 *Information Visualisation - Biomedical Visualisation*, pp. 9–14.
- 926 Werner, R., Ehrhardt, J., Schmidt, R., Handels, H., 2009a. Patient-specific finite element modeling of  
927 respiratory lung motion using 4d ct image data. *Medical Physics* 36, 1500–1511.
- 928 Werner, R., Ehrhardt, J., Schmidt-Richberg, A., Handels, H., 2009b. Validation and comparison of  
929 a biophysical modeling approach and non-linear registration for estimation of lung motion fields in  
930 thoracic 4d ct data, in: *SPIE Medical Imaging*, pp. 72590U–72590U.
- 931 West, J.B., Dollery, C.T., Naimark, A., 1964. Distribution of blood flow in isolated lung; relation to  
932 vascular and alveolar pressures. *Journal of Applied Physiology* 19, 713–724.
- 933 Wu, Z., Rietzel, E., Boldea, V., Sarrut, D., Sharp, G.C., 2008. Evaluation of deformable registration of  
934 patient lung 4dct with subanatomical region segmentations. *Medical Physics* 35, 775–781.
- 935 Yin, Y., Hoffman, E., Lin, C.L., 2010. Lung lobar slippage assessed with the aid of image registration, in:  
936 Jiang, T., Navab, N., Pluim, J.W., Viergever, M. (Eds.), *Medical Image Computing and Computer-  
937 Assisted Intervention MICCAI 2010. Springer Berlin Heidelberg. volume 6362 of Lecture Notes in*  
938 *Computer Science. book section 71*, pp. 578–585.
- 939 Yushkevich, P., Piven, J., Cody, H., Ho, S., Gee, J.C., Gerig, G., 2005. User-guided level set segmentation  
940 of anatomical structures with itk-snap.
- 941 Zhang, T., Orton, N.P., Mackie, T.R., Paliwal, B.R., 2004. Technical note: A novel boundary condition  
942 using contact elements for finite element based deformable image registration. *Medical Physics* 31,  
943 2412–2415.
- 944 Zhong, H., Kim, J., Li, H., Nurushev, T., Movsas, B., Chetty, I.J., 2012. A finite element method to  
945 correct deformable image registration errors in low-contrast regions. *Physics in Medicine and Biology*  
946 57, 3499–3515.